A Simple High-Precision 2-Port Vector Analyzer

JÁN LABUN[1], GABRIEL KALAPOŠ[1], MAREK ČEŠKOVIČ[1], PAVOL KURDEL[1], JÁN GAMEC[2], ALEXEY NEKRASOV[3], COLIN FIDGE[4], AND MIROSLAV LAŠŠÁK[5]

[1]Faculty of Aeronautics, Technical University of Košice, 041 21 Košice, Slovakia
[2]Faculty of Electrical Engineering and Informatics, Technical University of Košice, 042 00 Košice, Slovakia
[3]Institute for Computer Technologies and Information Security, Southern Federal University, 347922 Taganrog, Russia
[4]Faculty of Science and Engineering, Queensland University of Technology (QUT), Brisbane, QLD 4001, Australia
[5]Honeywell, Flight Controls Department in Brno, 627 00 Brno, Czech Republic

Corresponding author: Ján Gamec (jan.gamec@tuke.sk)

ABSTRACT This article presents a novel concept for a highly accurate and simple two-port vector signal analyzer. A current phase ratio measurement method is defined for one independent external signal with a restriction of the measuring range ±90 or $\pm180°$. The article presents a new way of phase ratio evaluation of two independent external signals with precise phase determination in a wide range from $0°$ to $360°$. The new functional blocks of the analyzer circuit element act as a four-position radio frequency (RF) switcher and an algorithm for phase determination is presented. Practical application and verification of the results achieved are demonstrated by measuring the phase directional radiation pattern of a complex object such as an aircraft fuselage.

INDEX TERMS Vector signal analyzer, measuring of phase ratios, radiation patterns.

I. INTRODUCTION

Vector signal and network analyzers have seen unprecedented progress in recent decades [1], [2]. The possibility of deep analysis of radio frequency (RF) signals is not limited to their amplitude and frequency but the phase area also provides additional information and enables deeper and more precise signal processing. This significantly expands the capabilities of RF technology [3]. There has been a significant tendency to develop new types of analyzers with quantitatively expanded performance [4] and qualitatively better parameters [5]. Better RF measurement equipment can help in the development of new RF technologies, which are applicable in various areas of society [6]–[8].

Vector signal analyzers (VSA) belong to a group of specific measurement devices that allow the evaluation of phase, which is required during the development of RF systems [9]. The other area where vector signal analyzers are helpful is solving electromagnetic compatibility problems, where a large amount of RF technology is concentrated in a small place [10]. High quality, high precision, special equipment

is produced only by a few companies around the world. These tools are extremely helpful and simplify research in RF technology, however, they are also expensive. Due to their high price, researchers sometimes use low-cost alternative equipment but with correspondingly limited functionality and bandwidth [11], [12].

This article presents the design, implementation, calibration, and measurement of a simple, low cost, and at the same time highly precise two-port vector signal analyzer. The goal of this design is to support direct phase measurement of the input signals.

Commonly used vector network analyzers evaluate the phase of the measured signal in relation to an internal (built-in) RF source [13], however they do not evaluate the phase ratio of two external RF signals. This is a limitation for the measurement of the directional radiation pattern of an antenna. In our research, airlines assigned the Department of Avionics, Faculty of Aeronautics, Technical University of Košice, the challenge of measuring the radiation pattern of an aircraft communication antenna. We investigated the task in a laboratory-based anechoic chamber on a reduced size model aircraft. As we discussed previously, the phase radiation pattern is important for the analysis of an antenna [14]. The shape

of the fuselage creating the artificial ground of the aircraft antenna affects the phase and the amplitude of the radiated signal in every direction [15], [16]. An aircraft antenna's radiation pattern is usually very fragmented and contains several significant maximums and minimums [17]. The environment close around the antenna, including the antenna's carrier (car, boat, airplane, building), significantly affects the antenna's radiation parameter. Nonetheless, achieving a reliable wireless connection is a requirement in every area of the public field (emergency services, air traffic control, space, and defense) [18], [21].

This article presents the design and calibration of a newly developed vector signal analyzer. The new VSA is based on an AD8302 phase comparator coupled with a special RF switcher for phase measurement adjustment. A proof-of-concept prototype device was set up for a 1.2 GHz frequency. A unique algorithm implemented in our VSA microcontroller evaluates the final phase ratio in a wide range of 0°–360°.

II. IC AD8302 AS A VECTOR SIGNAL ANALYZER

The basic design element of the vector signal analyzer is a phase comparator circuit AD8302. The standard circuit contains two identical logarithmic amplifiers (Fig. 1) integrated in a monolithic form. The design of the AD8302 printed circuit board can be seen in Fig. 2.
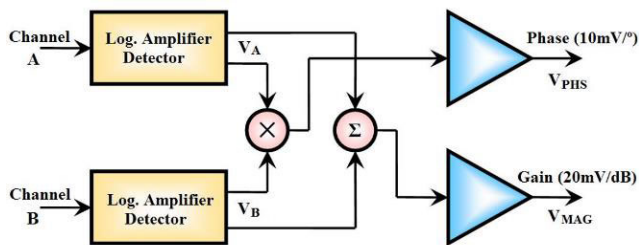
FIGURE 1. Phase comparator circuit AD8302.
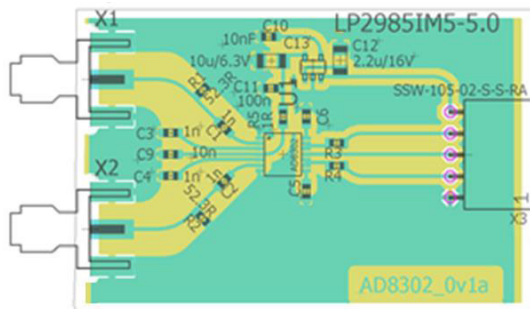
FIGURE 2. Design of the AD8302 PCB.

Every channel of the circuit can measure a signal in the range of 60 dB from very low frequencies up to 2.5 GHz. The amplitude gain can be computed as follows [19]

$$V_{MAG} = V_{SLP} \cdot \log(V_A/V_B) + V_{CP}, \tag{1}$$

where V_A is the reference signal and V_B is a measured signal connected to the input ports of the AD8302 circuit, V_{CP} is

the center point, defined as the V_{MAG} output value at the difference level of 0 dB, and V_{SLP} and V_{CP} are the design options linked to the temperature changing reference.

The AD8302 measures the phase difference between two signals. Each of the individual logarithmic amplifiers has a limited output. These signals are input to a phase detector with precise symmetry with respect to the dual input within the range of 180°. The output phase ratio V_{PHS} is given by the following equation

$$V_{PHS} = \pm V_\Phi(\Phi - 90°) + V_{CP}, \tag{2}$$

where V_Φ is the scaling voltage at the phase output, Φ is the phase difference between the two inputs, and the +/− sign depends on the quadrant of the 180° range.

The AD8302 circuit behaves as a single-chip vector signal analyzer. The RF detector and the microcontroller part are in a separate shielded case. The shielding is made from 0.3 mm thick copper sheet. The case has two sections shielded from each other. The microcontroller part of the circuit is in the rear, Section A, which contains a single-chip ATM328 processor, an 8-bit microcontroller with an operating frequency of 8 MHz. The data output of the microcontroller is connected to the USB output via an RS232 serial converter. Figure 3 shows the half-exposed RF detector and microcontroller module.
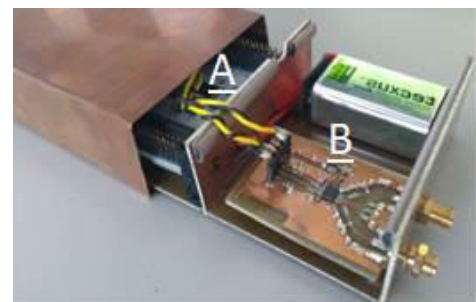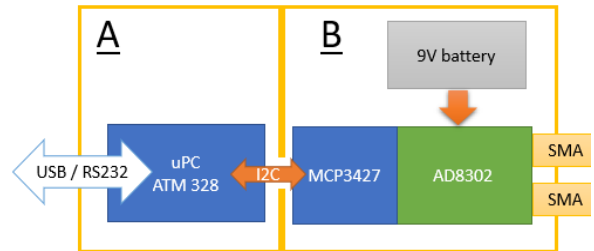
FIGURE 3. Final design of the vector signal analyzer.

Section B contains the AD8302 RF detector circuit. It is a single-chip vector signal analyzer that has two RF inputs and two DC information outputs. The outputs are sampled by a 16-bit MCP3427 ADC converter.

A. AMPLITUDE CALIBRATION OF AD8302

A block diagram of the workstation for amplitude calibration of the AD8302 circuit is shown in Fig. 4. The output from the RF signal generator is divided by a directional coupler into two branches. The RF signal from the output of the
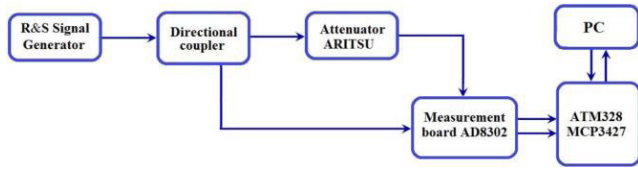
FIGURE 4. Block diagram of the workstation for amplitude calibration.

directional coupler's first branch is 0 dBm and the output from the coupler's second branch is attenuated by –30 dB. An attenuator circuit is included in the first branch. The RF signal of each branch is connected separately to one of the AD8302 circuit's inputs. The second branch's RF signal output, attenuated to the level of –30 dBm, will have a constant value during measurement.

During the calibration measurement, the level of the RF signal from the first branch is attenuated in a range from 0 dBm to –60 dBm with a step of –1 dB. Each change in the RF signal's level is recorded.

The AD8302 circuit's amplitude transfer characteristic at an operating frequency of 1.2 GHz is presented in Fig. 5. A 4th order polynomial was used for approximation of the amplitude transfer function. The calibration can be used in a range from ±25 dB at the reference signal level of –30 dBm.
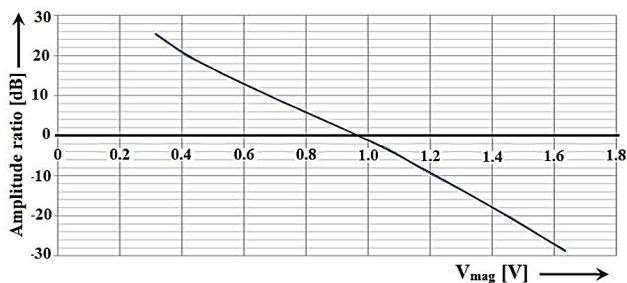

FIGURE 5. Amplitude transfer function of the AD8302 at 1.2 GHz.

B. PHASE CALIBRATION OF THE AD8302

For a precise phase calibration of the circuit, a linearly adjustable coaxial line with an air dielectric was developed. The coaxial line consists of 3 brass tubes, one brass rod, 3 dielectric spacers, and 2 SMA connectors. The adjustable coaxial line's design is shown in Fig. 6. Its effective range is 0–220 mm. This range represents 88% of the wavelength at a frequency of 1.2 GHz (or an angular range of 0°–316.8°).
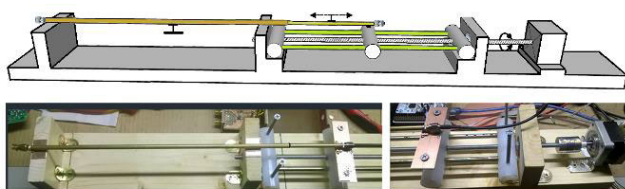

FIGURE 6. Model of the linear adjustable coaxial line.

Our adjustable coaxial line was verified using an R&S FSH8 network analyzer. The phase shift of the adjustable coaxial line was set to 0° at the starting point of the measurement. Subsequently, the network analyzer measured a phase shift in the range from –180° to +180°.

More than one period of phase change at a frequency of 2.4 GHz and less than one period of phase change at a frequency of 1.2 GHz was observed during a mechanical shift of the adjustable coaxial line over the effective range. From the measured results it can be seen in Fig. 7 that the phase change is not linear, especially at 2.4 GHz. This observation can be explained by an impedance mismatch at the higher frequency.
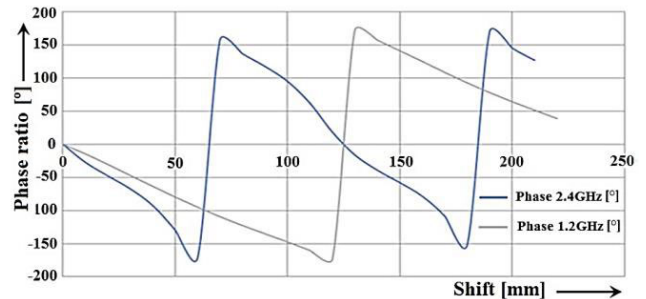

FIGURE 7. Phase characteristic of the adjustable coaxial line measured by the R&S FSH8.

The block diagram of the workstation for the AD8302 circuit's phase calibration is shown in Fig 8. A dual directional coupler was used in the measurement as it provides two separate RF signal sources with the same phase and attenuated by –30 dB. These two output RF signals are connected to input ports of the AD8302 vector signal analyzer, with the adjustable coaxial line connected in one branch.
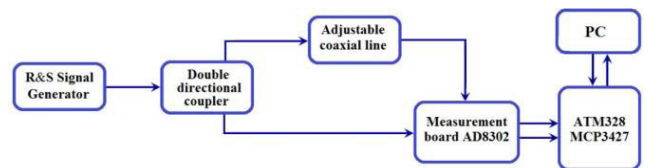

FIGURE 8. Block diagram of the workstation for phase calibration.

The phase characteristic of the AD8302 circuit is presented in Fig. 9. The orange curve shows the data from the AD8302, the grey dotted curve shows the data from the R&S FSH8 network analyzer, and the yellow curve is the calculated correction. The blue curve corresponds to the data from the AD8302 with correction applied. A 4th order polynomial with an accuracy of 20 digits was used for the correction curve approximation.

To increase the overall accuracy, the correction curve was divided into 3 sections: [20° 40°], [40° 140°] and [140° 160°]. The AD8302 is precise enough only in the linear range of the phase characteristic [40° 140°]. The biggest disadvantage is the mirrored characteristic resulting in an inability to distinguish whether the phase shift is in a positive or negative direction in a range of ±180°.
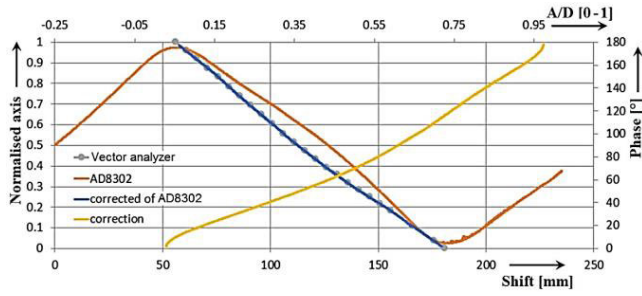
FIGURE 9. Phase characteristic of the AD8302.

III. VSA WITH THE RF SWITCHER

To obtain high phase measurement accuracy in the range 0°–360°, it is required to move the measurement point into the linear section of the phase characteristic 40°–140°. To do this, the input reference signal is phase shifted by a known value. The phase shift of the reference signal has to be at a minimum of 40° and a maximum of 140° to allow measurement in the wide range 0°–360°.

The required phase shift was created by two four-channel RF switches (SW1 and SW2) connected via 4 microstrip lines (RF1, RF2, RF3 and RF4) of different known lengths. The RF switcher diagram is illustrated in Fig. 10 and its final realization is presented in Fig. 11.
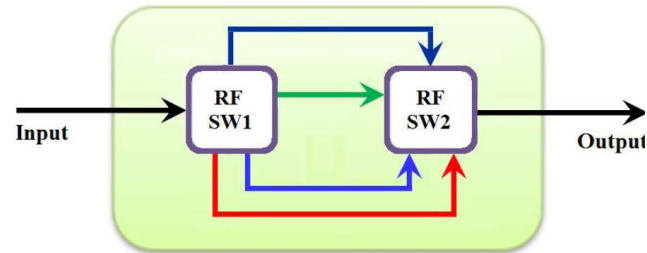

FIGURE 10. RF switcher block diagram.

The lengths of the microstrip lines are in the relation RF1 < RF2 < RF3 < RF4, where RF1 is the shortest and RF4 is the longest. The length of the RF1 line is determined by the mechanical design of the RF switcher's entire circuit. To achieve the lowest attenuation, it should be set as short as possible. The RF1 line's length can be considered as the basic length. The length of RF2 is equal to RF1 + ΔL, where ΔL is the length of line that will create a known phase shift in the required range, minimum of 40° and maximum of 140°.

The theoretical upper limit of the measurable phase shift using only two microstrip lines RF1 and RF2 is from 40° to 140° plus the known phase shift of RF2. Using all four microstrip lines, including RF3 and RF4, it is possible to increase the maximum measurable phase shift. For the lengths RF3 = RF1 + 2 ×ΔL and RF4 = RF1 + 3 ×ΔL, the maximum measurable phase shift is increased to a range from −180° to +180°, or 0°–360°. This approach also allows phase shift measurement in the so-called mirror region.
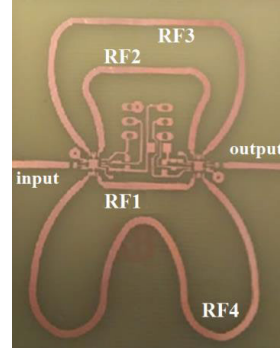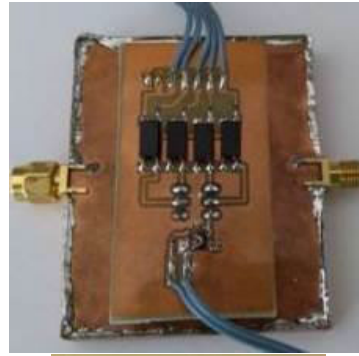

FIGURE 11. RF switcher realization.

Input parameters for calculating the geometric dimensions of the lines for the reference signal's phase shift were:
- the material of the PCB, FR-4, $\varepsilon_r = 4.3$,
- 1/sqrt (ε_r) = 0.482,
- the design operating frequency of 1.2 GHz, and
- the phase shift planned to be achieved with ΔL of 90°.

An RF HMC7992 switch circuit was used in the developed RF switcher to allow a phase shift of the reference signal. The RF switcher was designed so that only one line is active at a time and the other three inactive lines are terminated with a 50 Ω impedance. A digital TTL signal is used to select the active line. Internal attenuation of the switch circuit is in the range –0.5 to –1.5 dB at a frequency range of 0.1–6 GHz. The switcher's inactive lines have an isolation of –60 to –40 dB in the same frequency range.

Table 1 shows the lengths of the microstrip lines and the corresponding measured phase shift of the manufactured RF switcher prototype at an operating frequency of 1.2 GHz.

TABLE 1. Parameters of the RF lines.

	RF1	RF2	RF3	RF4
LENGTH [MM]	17.45	48.8	79.8	110.9
F$_{MAX}$ [GHZ]	17.17	6.14	3.75	2.7
MEASURED PHASE SHIFT	0º	76.5º	149.5º	224.2º

The planned phase shift for the length of ΔL was 90°, while the manufactured RF switcher prototype had a phase shift of 76.5°. This difference was caused by inaccuracy during the manufacturing process but does not affect the final accuracy of the phase shift measurement.

The measured phase shift of the RF switcher with the AD8302 circuit demonstrates the expected functionality and confirms that the design increases the operating range of the phase comparator.

The practical integration of the RF switcher into the measurement chain for evaluation of its performance in the whole phase range was executed with the adjustable coaxial line (Fig. 12).
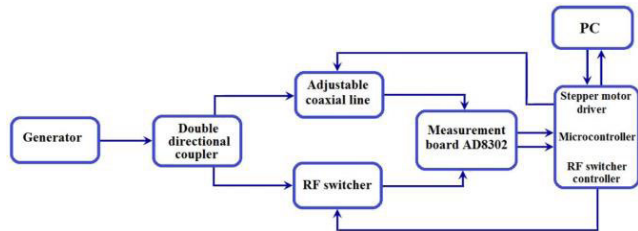

FIGURE 12. RF switcher realization.

A frequency of 1.2 GHz was set at the signal generator, and its output was connected to a double directional coupler to create two identical RF signals. The first signal was routed to the AD8302 phase comparator is first input via the adjustable coaxial line. The second signal was routed to the comparator's second input via the 4-channel RF switcher.

The microcontroller drove the RF switcher to select the active line and measured the phase shift. Once all four lines were measured, the adjustable coaxial line was shifted by 1mm. Measured data was transferred to a PC for evaluation (Fig. 13). The horizontal axis represents the shift of the adjustable coaxial line from 0 mm to 220 mm. The vertical axis represents the phase ratio in degrees; data was used only in the range 40°–140°. The phase ratio can be calculated up to three times in every step of the shift.
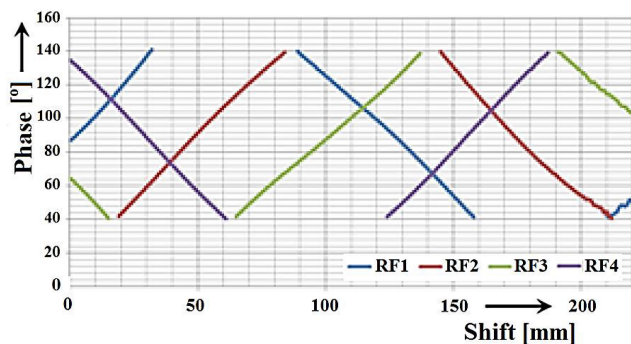

FIGURE 13. Measured phase ratios.

The final product, designated JVA-360, was installed into a standard 19'' rack as shown in Fig. 14. The device consists of 4 functional blocks. Two independent DC voltage sources (A) of 9 V and 5 V are galvanically isolated from the main power supply of 230 V. An additional differential coil, and ceramic and electrolytic capacitors are used as an EMC filter connected to the outputs of the voltage sources. The output voltage is distributed by a shielded twisted pair. A USB data connection is 1000 V isolated with a commercial DC/DC converter (B) of 250 mA, and 5 V powered from the PC.
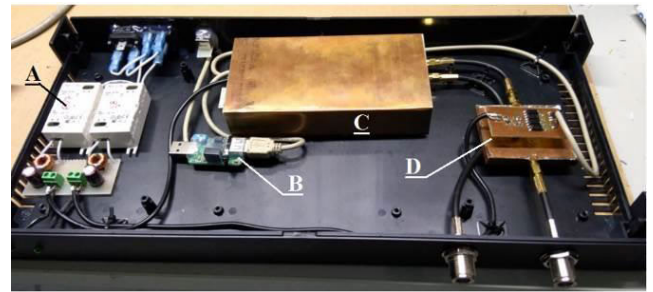

FIGURE 14. Final view of the JVA-360 vector analyzer.

The AD8302's first RF input (C) is routed directly to connector 1 of the front panel via a coaxial line. The AD8302's second RF input passes through the RF switch (D) to connector 2 of the front panel. A simplified block diagram of the JVA-360 wiring is shown in Fig. 15.

FIGURE 15. Block diagram of the JVA-360's wiring.

The phase shift's final value is determined as a function of four measured values from the RF switcher (RF1, RF2, RF3, RF4) and the phase shift constants of the RF switcher lines. The algorithm for calculating the final value of the phase shift in the range of 0°–360° was developed and implemented in C programming language code, using the ATM328 microcontroller.

Table 2 summarizes all possible states that can occur when measuring phase ratios using the RF switcher. Those states' identification is presented in Fig. 16. Following Table 2, 24 different states are possible, and special logic is used to determine the current state. It decides whether the measured phase shift is in the range 40°–90° (highlighted yellow), is in the range 90°–140° (highlighted green), or cannot be evaluated (highlighted white) while using the selected active line for the measurement.
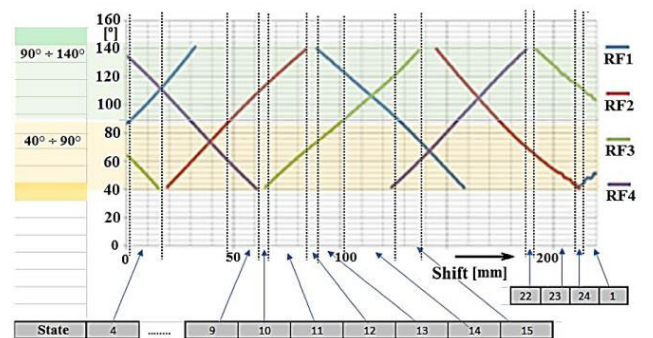

FIGURE 16. The 24-state identification.

When all four lines of the RF switcher were measured, the current state from Table 2 was identified by the algorithm.

TABLE 2. State definition for the phase calculation algorithm.

No.	Real Phase	Measured Phase			
		RF1	RF2	RF3	RF4
1	0.3	40		109	
2	20.3	60		89	
3	44.1	84		65.6	140
4	51.1	91		58.6	133
5	70.1	110			114
6	77.1	117	40.5		107
7	94.1	134	57.5		90
8	101.1		64.5		83
9	127.1		90.5		57
10	145		108.5		
11	150		113.5	40.4	
12	177.9			68.4	
13	180	140		70.4	
14	200	120		90.4	
15	224.9	95		115.4	40.4
16	229.9	90		120.4	45.4
17	250.8	69			66.4
18	256.7	63	140		72.4
19	274.7	45	122		90.4
20	280.6		116		96.4
21	306.6		90		122.4
22	325.5		71		
23	329.5		67	140	
24	357.5				112

TABLE 3. Unique formulae for calculation of the phase from the state.

RF1=**A**; RF2=**B**; RF3=**C**; RF4=**D**; 76.45=**E**; 149.55=**F**; 224.19=**G**;

1	PHASE $= [(A + F - C)/2] - 40$
2	PHASE $= [(A + F - C)/2] - 40$
3	PHASE $= [(A + F - C + G - D)/3] - 40$
4	PHASE $= [(A + F - C + G - D)/3] - 40$
5	PHASE $= [(A + G - D)/2] - 40$
6	PHASE $= [(A + E + B + G - D)/3] - 40$
7	PHASE $= [(A + E + B + G - D)/3] - 40$
8	PHASE $= [(E + B + G - D)/2] - 40$
9	PHASE $= [(E + B + G - D)/2] - 40$
10	PHASE $= (E + B) - 40$
11	PHASE $= [E + B + F + C)/2] - 40$
12	PHASE $= (F + C) - 40$
13	PHASE $= [(360 - A + F + C)/2] - 40$
14	PHASE $= [(360 - A + F + C)/2] - 40$
15	PHASE $= [(360 - A + F + C + G + D)/3] - 40$
16	PHASE $= [(360 - A + F + C + G + D)/3 - 40$
17	PHASE $= [(360 - A + G + D)/2] - 40$
18	PHASE $= [(360 - A + 360 - B + E + G + D)/3] - 40$
19	PHASE $= [(360 - A + 360 - B + E + G + D)/3] - 40$
20	PHASE $= [(360 - B + E + G + D)/2] - 40$
21	PHASE $= [(360 - B + E + G + D)/2] - 40$
22	PHASE $= (360 - B + E) - 40$
23	PHASE $= [(360 - B + E + 360 - C + F)/2] - 40$
24	PHASE $= (360 - B + F) - 40$
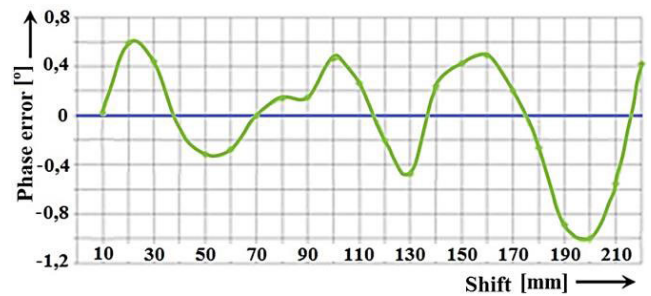
FIGURE 17. Measured phase error of the JVA-360.

The algorithm for calculating a specific phase is based on a combination of the presence (absence) of measured outputs in individual channels, on the number of measured outputs in a given section and from the size of the measured values in the range ($40° - 90°$ or $90° - 140°$). This combination of measured parameters determines in which section of the measurement we are located. Unique formulae, presented in Table 3, must be applied for each state to calculate the instantaneous phase shift in the range $0° - 360°$.

The following substitution was used to simplify the mathematical interpretation of the calculation.

Measured values $40° - 140°$:   Constants:

RF1 $\rightarrow$ A

RF2 $\rightarrow$ B   RF1_RF2 $= 76.5° \rightarrow$ E

RF3 $\rightarrow$ C   RF1_RF3 $= 149.5° \rightarrow$ F

RF4 $\rightarrow$ D   RF1_RF4 $= 224.2° \rightarrow$ G

Figure 17 illustrates the phase difference between the measurement of the phase shift using the R&S FSH8 network

analyzer and our JVA-360 device. The phase error was in the range from $+0.6°$ to $-1°$. The JVA-360 measures the amplitude difference in the range ± 25 dB against the reference signal -30 dBm and the phase difference in the range of $0° - 360°$ at a rate of 50 measurements per second.

IV. EXPERIMENTAL MEASUREMENTS USING THE AIRCRAFT MODEL

A reliable way to check the correct operation of our JVA-360 is measurement of an antenna's directional pattern with a known amplitude and phase radiation. A simple asymmetrical unipole antenna with an artificial ground of circular shape was designed and manufactured. The unipole measurement was performed in the horizontal plane (φ) and in the vertical plane (ϑ) in an anechoic chamber. The theoretical

unipole antenna radiation pattern was modeled in FEKO simulation software, for comparison with measured data.

The experimental results are summarized as follows:

- Both measured characteristics (amplitude and phase) highly correlate to the radiation pattern from the simulation. Nonsignificant differences can be explained by the precision of the simulation tool against the manufactured unipole antenna.
- Small differences are in the hemispheric area where the antenna is powered via the coaxial line. Mechanical elements and the power cable were not taken into account in the simulation.

Since the correct operation of the JVA-360 was proven by the unipole antenna measurement, the next step was the measurement of an aircraft antenna model. An Embraer Phenom scaled model (1:10) with its surface coated by a conductive aluminum foil was used (Fig. 18). Communication frequencies used in civil aviation are spread in the range of 118–137 MHz. To maintain the ratio of the wavelength of the operating frequency and the aircraft's physical dimensions, while comparing the aircraft model (1:10) and the real aircraft, the frequency used for the aircraft model (1:10) has to be ten times higher, which drove the 1.2 GHz calibration frequency for the JVA-360.
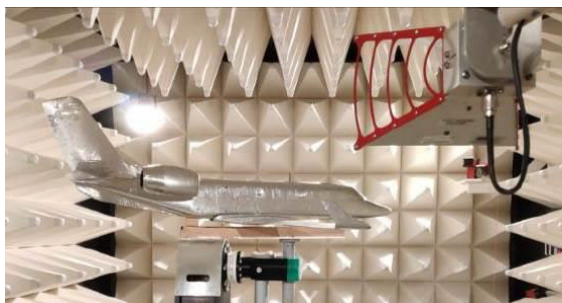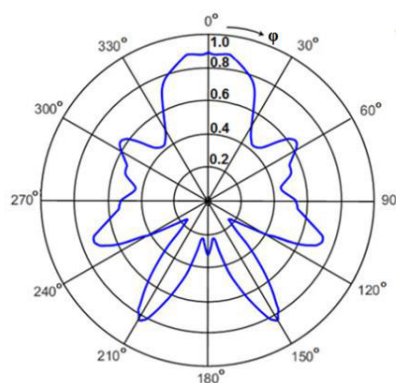

FIGURE 18. Measurements of the aircraft model in the horizontal plane.

For the demonstration purposes, the aircraft's antenna radiation patterns were measured in one antenna position, located at the top center of the aircraft model (Fig. 19b). The measured aircraft antenna model radiation patterns are illustrated in Fig. 19.

The shape and size of the fuselage, including the position of the antenna and the operating frequency, creates the fragmented shape of the amplitude and the phase radiation pattern of the communication antenna in polar coordinates. Seven significant local maximums and seven minimums can be observed in the measured radiation patterns.
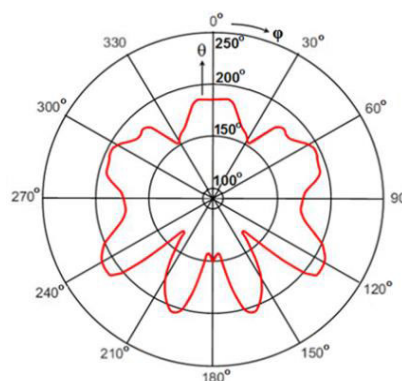
The measurement of the radiation pattern of the aircraft's communication antenna was mainly driven by the need to explain several field issues reported by aircraft operators. Radio communication with the aircraft at the specific angle of 130° rotation was hardly achievable even with direct visibility without obstacles. However good communication quality was achieved in the directions where the aircraft antenna is shadowed by the wing (60°, 110°), by the elevator (150°)

a)

b)

c)

FIGURE 19. Measured radiation pattern of the aircraft model in the horizontal plane (φ). (a) Amplitude radiation pattern of the aircraft antenna in linear scale. (b) Rotation of the aircraft model at the manipulator, φ angle. (c) Phase radiation pattern of the aircraft antenna.

or by the fuselage (0°) [20]. We thus see that radio connection quality depends on both the amplitude and the phase radiation patterns, which are presented in Fig. 19. The JVA-360 uses only one coaxial line to evaluate the amplitude of the transmitting antenna signal, without mutual interconnection of the other lines.

V. CONCLUSION

The amplitude radiation pattern is a standard parameter for the specification of an antenna. However, a particularly important parameter that is not very often a subject of interest is the phase radiation pattern. The phase is an inseparable part

of the signal description. Normally complex and expensive tools must be used for phase ratio measurement under special laboratory conditions.

Our novel prototype equipment, the JVA-360, which can be used for the measurement of both the phase ratio and the amplitude ratio, was presented in this paper. The prototype is of low cost and quite simple design. It can be replicated with common laboratory equipment. The linear adjustable coaxial line was developed and used as a supporting tool for shifting the phase during the calibration of the phase ratio. The developed RF switcher was used for phase shifting of the reference signal by four different known values to extend the phase measurement range. The four measured values of the phase shift were used by an algorithm implemented in the microcontroller for the final phase calculation.

The accuracy of the phase ratio measured by the JVA-360 was evaluated by a high precision R&S FSH8 network analyzer using the developed adjustable coaxial line. The calculated phase error was in the range +0.6° to −1°, which is 0.3% of the angular range of 0°–360°. Our prototype JVA-360 was calibrated at a frequency of 1.2 GHz, and its frequency range is in the band from 1.0 to 1.8 GHz. The extension of this band is limited only by the hardware solution of the RF switcher.

The major benefit of our JVA-360 device is the ability to measure both the amplitude and the phase radiation pattern of an antenna. The proper functionality of the prototype JAV-360 was demonstrated on a scale aircraft model equipped with a typical communications antenna.

The prototype JVA-360 has the potential to be converted to a vector network analyzer. At the very least, it would be desirable to supplement this device with directional couplers and an internally calibrated signal source.

REFERENCES

[1] P. Meaney, A. Hartov, S. Bulumulla, T. Raynolds, C. Davis, F. Schoenberger, S. Richter, and K. Paulsen, "A 4-channel, vector network analyzer microwave imaging prototype based on software defined radio technology," *Rev. Sci. Instrum.*, vol. 90, no. 4, Apr. 2019, Art. no. 044708, doi: 10.1063/1.5083842.

[2] W. Lowdermilk and F. Harris, "Vector signal analyzer implemented as a synthetic instrument," in *Proc. IEEE Autotestcon*, Sep. 2007, pp. 157–166, doi: 10.1109/AUTEST.2007.4374215.

[3] H. Zhang, S. Krooswyk, and J. Ou, "Measurement and data acquisition techniques," in *High Speed Digital Design*. San Mateo, CA, USA: Morgan Kaufmann, 2015, pp. 199–219, ch. 5, doi: 10.1016/B978-0-12-418663-7.00005-8.

[4] Á. Szülő, J. Orbán, and G. Mikó, "Development of a multichannel vector network analyzer for 'in situ' Meas. radar antennas," in *Proc. Conf. Microw. Techn. (COMITE)*, Pardubice, Czech Republic, Apr. 2015, pp. 1–4, doi: 10.1109/COMITE.2015.7120317.

[5] J. Yu and M.-H. Ka, "Precision near-field reconstruction in the time domain via minimum entropy for ultra-high resolution radar imaging," *Remote Sens.*, vol. 9, no. 5, p. 449, May 2017, doi: 10.3390/rs9050449.

[6] M. Hefnawi, J. Bray, J. Bathurst, and Y. Antar, "MIMO radar using a vector network analyzer," *Electronics*, vol. 8, no. 12, p. 1447, Dec. 2019.

[7] M. Macdonell and J. Scott, "Development and basic calibration of an acoustic vector network analyser," in *Proc. Electron. New Zealand Conf.*, Christchurch, New Zealand, Dec. 2017, pp. 4–6. [Online]. Available: https://www.researchgate.net/publication/321807658_Development_and_Basic_Calibration_of_an_Acoustic_Vector_Network_Analyser/stats

[8] K. Draganová, K. Semrad, L. Fozo, M. Spodniak, and R. Jurc, "Methodology for structural analysis of hyperelastic materials with embedded magnetic microwires," *Metalurgija*, vol. 59, no. 3, pp. 389–392, Oct. 2020. [Online]. Available: https://hrcak.srce.hr/index.php?show=clanak&id_clanak_jezik=34421

[9] A. Zaidi, F. Athley, J. Medbo, U. Gustavsson, G. Durisi, and X. Chen, "Propagation & channel modeling," in *5G Physical Layer*. New York, NY, USA: Academic, 2018, pp. 35–85, ch. 3, doi: 10.1016/B978-0-12-814578-4.00008-4.

[10] A. Manara, "Measurement of material shielding effectiveness using a dual TEM cell and vector network analyzer," *IEEE Trans. Electromagn. Compat.*, vol. 38, no. 3, pp. 327–333, Aug. 1996. [Online]. Available: https://ieeexplore.ieee.org/document/536062, doi: 10.1109/15.536062.

[11] T. Hart. *W5QJR—The BOOK on EH Antenna*. pp. 10–12. Accessed: Jul. 26, 2020. [Online]. Available: http://kambing.ui.ac.id/onnopurbo/orari-diklat/teknik/antenna/eh-antenna/eh-antenna-book/EH%20antenna%20-%20the%20Book.pdf

[12] J. Verhaevert and P. V. Torre, "A low-cost vector network analyzer: Design and realization," in *Proc. Loughborough Antennas Propag. Conf. (LAPC)*, Loughborough, U.K., Nov. 2017, pp. 1–5. [Online]. Available: https://ieeexplore.ieee.org/document/8363957, doi: 10.1049/cp.2017.0225.

[13] *R&S®ZVL Vector Network Analyzer. Operating Manual.* Accessed: Oct. 28, 2020. [Online]. Available: https://cdn.rohde-schwarz.com/pws/dl_downloads/dl_common_library/dl_manuals/gb_1/z/zvl_1/ZVL_Operating_en_09.pdf

[14] G. Kalapoš, M. Krchňák, M. Češkovič, J. Labun, M. Schreiner, and T. Moravec, "The effect of shape of artificial ground on antenna radiation pattern," *OUR SEA: Int. J. Maritime Sci. Technol.*, vol. 65, no. 3, pp. 157–163, Oct. 2018, doi: 10.17818/NM/2018/3.5.

[15] B. Turetken, F. Ustuner, and A. Dagdeviren, "Numerical and experimental study of F-4 aircraft antenna patterns," *Int. J. Electron.*, vol. 94, no. 3, pp. 293–301, Mar. 2007, doi: 10.1080/00207210701223378.

[16] T. M. Macnamara, *Introduction to Antenna Placement and Installation*. Hoboken, NJ, USA: Wiley, 2010, p. 410, doi: 10.1002/9780470686874.

[17] A. I. Mackenzie, "EM modeling of far-field radiation patterns for antennas on the GMA-TT UAV," *Proc. SPIE*, vol. 9460, pp. 1–8, Apr. 2015. [Online]. Available: https://ntrs.nasa.gov/archive/nasa/casi.ntrs.nasa.gov/20150010967.pdf

[18] M. Blistanova, J. Blažek, P. Blistan, J. Reitšpís, and P. Havaj, "Support for Protection of the Large Object Using UAVs," *Adv. Mil. Technol.*, vol. 11, no. 2, pp. 227–237, Dec. 2017. [Online]. Available: http://aimt.unob.cz/articles/16_02/1159.pdf

[19] Analog Devices. (2002). *Datasheet AD8302: RF/IF Gain and Phase Detector.* [Online]. Available: https://www.analog.com/media/en/technical-documentation/data-sheets/ad8302.pdf

[20] M. Pavlík, L. Kruželák, L. Lisoň, M. Mikita, S. Bucko, M. Špes, M. Ivančák, B. Dolník, and J. Zbojovský, "The mapping of electromagnetic fields in the environment," *Acta Technica Corviniensis: Bull. Eng.*, vol. 10, no. 2, pp. 107–110, Jun. 2017. [Online]. Available: http://acta.fih.upt.ro/ACTA-2017-2.html

[21] T. Vaispacher, R. Bréda, and R. Andoga, "Integration architecture design for implementation of a vector magnetometer on board of unmanned vehicle," in *Proc. IEEE 15th Int. Symp. Comput. Intell. Informat. (CINTI)*, Budapest, Hungary, Nov. 2014, pp. 483–489, doi: 10.1109/CINTI.2014.7028724.

JÁN LABUN received the diploma degree in aircraft instruments technology and the Ph.D. degree in aviation technics from CVUT Prague with a focus on radionavigation systems, in 1989 and 1999, respectively.

He received the title Associate Professor of electronics from the Technical University of Košice in 2010. Since 2016, he has been working as an Associate Professor with the Department of Avionics, Faculty of Aeronautics. He is the author of eight patents and also a reviewer of MDPI journal. His research interests include antenna modeling and simulation, both airborne and ground based radar devices and radar altimeters.

GABRIEL KALAPOŠ received the diploma degree in sensorics and Avionic systems and the Ph.D. degree in aviation and industrial electronic systems (electro engineering) from the Faculty of Aeronautics, Technical University of Košice, in 2014 and 2020, respectively.

From 2016 to 2018, he had been working as a Research and Development Engineer with Vossloh Schwabe Deutschland GmbH, Trnava, Slovakia, where he applied for a patent method for evaluating a radar signal and system. Since 2018, he has been working as a System Engineer with the Honeywell, CNS Data-Link Department in Brno, Czech Republic. His research interests include antenna modeling and simulation, RF radar solutions, VHF antenna radiation pattern, and other areas in aerospace.

MAREK ČEŠKOVIČ received diploma degree in sensorics and Avionic systems and the Ph.D. degree in aviation and industrial electronic systems (electro engineering) from the Faculty of Aeronautics, Technical University of Košice, in 2011 and 2014, respectively.

Since 2014, he has been working as an Assistant Professor with the Technical University of Košice. He is currently a Technical Director of the Laboratory of Airborne Antenna Equipment and a member of the Laboratory of Intelligent Control Systems of Jet Engines. He has been a Reviewer in IEEE SAMI, CINTI, MOSATT, and NTAD conferences. His research interests include antenna modeling and simulation, RF radar solutions, VHF antenna radiation pattern, and other areas in aerospace.

PAVOL KURDEL finished the Military Aviation Academy in Košice, Slovakia. He received the engineer degree in electronics in 2000, and the Ph.D. degree in electronics from the Technical University of Košice, in 2011.

In 2016, he received the title of Associate Professor of electronics from the Technical University of Košice. From 2011 to 2014, he worked as an Assistant Professor with the Department of Avionics, Faculty of Aeronautics, Technical University of Košice. From 2014 to 2017, he was the Vice-Dean of the Faculty of Aeronautics. Since 2017, he has been working as an Associate Professor. From 2015 to 2017, he was a member of the Supervisory Board of Košice International Airport. He was a member of international projects within the EU, where the most important was the construction of a research and development facility for aircraft antenna research. He is the author of 110 publications, including monographs, textbooks, patents, and articles indexed in WoS – Current Contents Connect and Scopus. He is a holder of a medal and awards from the Minister of Defense of the Slovak Republic and the Faculty of Aeronautics. His research interests include electronic aircraft systems, traffic ergonomic systems management, airport processes, and remote sensing.

JÁN GAMEC was born in Stul'any, Slovakia, in 1960. He received the degree *(summa cum laude)* from the Technical University of Košice, Slovakia, in 1985, with specialization in radioelectronics, and the Ph.D. degree in radioelectronics from the Technical University of Košice, in 1995.

He is currently an Associate Professor with the Department of Electronics and Multimedia Communications, Faculty of Electrical Engineering and Informatics, Technical University of Košice. He holds one patent. His research interests include digital image processing, UWB radar signal processing, low-profile antennas for UWB radars, and remote sensing.

ALEXEY NEKRASOV received the diploma degree in radio engineering and the Ph.D. degree in technical science from the Taganrog State University of Radio Engineering (TSURE), Taganrog, Russia, in 1991 and 1998, respectively.

He received the academic title of Associate Professor from TSURE, in 2000. From 1991 to 1999, he was an Assistant Professor with TSURE. Since 1999, he has been an Associate Professor with the Southern Federal University (formerly TSURE). Since 2016, he has also been as a Senior Scientist with Saint Petersburg Electrotechnical University, Russia. He is currently with the Technical University of Košice, Slovakia. His research interests include sea and land remote sensing from aircraft and satellites, oceanography, sea winds, scattering from rough surfaces, radar system design, and information security. He has been an Expert of the Russian Academy of Sciences, the Russian Science Foundation, the Fulbright Program in Russia, a recipient of 24 international grants and awards, and a Reviewer of IEEE Transactions on Geoscience and Remote Sensing, IEEE Geoscience and Remote Sensing Letters, IEEE Antennas and Wireless Propagation Letters, *Remote Sensing*, *Atmosphere*, *Climate*, *Symmetry*, *Journal of Marine Science and Engineering*, *IET Radar, Sonar & Navigation*, *IET Image Processing*, and *ISPRS International Archives of the Photogrammetry, Remote Sensing and Spatial Information Sciences*.

COLIN FIDGE received the Ph.D. degree in computer science from Australian National University, in 1990. Since 2005, he has been a Full Professor with the Queensland University of Technology, where he is currently supervising research into analysis of network traffic and device logs, and modeling of control system behavior. His research interests include modeling and analysis of high-integrity and computer-based systems. He has extensive experience in leading major research projects, including 19 grant-funded projects, and six industry-funded projects. He has conducted research on the analysis of security-critical communications devices for the Australian Signals Directorate and safety-critical control systems for the Australian electricity distribution industry.

MIROSLAV LAŠŠÁK received the Diploma degree in sensorics and avionic systems and the Ph.D. degree in aviation and industrial electronic systems (electro engineering) from the Faculty of Aeronautics, Technical University of Košice, in 2011 and 2014, respectively.

Since 2014, he has been working as a System Engineer with the Honeywell, Flight Controls Department in Brno, Czech Republic. He has been a Reviewer in Acta Polytechnica Hungarica, and IEEE SAMI, CINTI, and INES conferences. His research interests include testing and calibration of inertial sensors, modeling and controls (camera gimbal and servovalve of jet engine), and other areas in aerospace.

● ● ●